Diurnal Variability of the Planetary Albedo: An Appraisal with Satellite Measurements and General Circulation Models

G. L. POTTER,* R. D. CESS,** P. MINNIS,† E. F. HARRISON† AND V. RAMANATHAN@

* *Lawrence Livermore National Laboratory, University of California, Livermore, California*
** *Laboratory for Planetary Atmospheres Research, State University of New York, Stony Brook, New York*
† *Atmospheric Sciences Division, NASA Langley Research Center, Hampton, Virginia*
@ *Department of the Geophysical Sciences, University of Chicago, Chicago, Illinois*

(Manuscript received 20 May 1987, in final form 22 September 1987)

ABSTRACT

This study addresses two aspects of the planetary albedo's diurnal cycle, the first of which refers to directional models of the planetary albedo. It is found that even for clear regions there appear to be deficiencies in our knowledge of how to model this quantity. Over land surfaces, for example, Nimbus-7 data for the directional planetary albedo compare best with model calculations for which a Lambertian surface is assumed, despite ample evidence that the albedo of land surfaces is dependent upon solar zenith angle. Similarly, over ocean surfaces both GOES and Nimbus-7 data produce a weaker dependence of the planetary albedo upon solar zenith angle than would be suggested by model calculations.

The second aspect of the study concerns a comparison of the diurnal amplitude factor, defined as the ratio of the diurnally averaged planetary albedo to that at noon, between two general circulation models (GCMs) and measurements made from a geostationary satellite (GOES). While these comparisons indicate reasonable consistency between the GCMs and the satellite measurements, this is due in part to compensating differences, such as an underestimate in cloud amount by a GCM being compensated for by a corresponding underestimate of the diurnal amplitude factor for overcast regions. The comparisons further underscore difficulties associated with converting local-time albedo measurements, as made from sun-synchronous satellites, to diurnally averaged albedos.

1. Introduction

Although earth radiation budget measurements from satellites have been made for over a quarter of a century, there still remains a particularly vexing problem. This concerns the determination of the diurnally averaged planetary albedo from measurements that are often restricted to very limited time sampling. To cite one example, the earth radiation budget data determined from the NOAA scanning radiometers (Gruber and Winston, 1978) refer to a sun-synchronous orbit with an 0900 equator crossing time, and it was simply assumed that this local-time albedo measurement represented the diurnally averaged albedo. While the 0900 crossing time was dictated by completely different reasons, studies employing geostationary satellites (Minnis and Harrison, 1984; England and Hunt, 1984) and a general circulation model (Ramanathan, 1987), coincidentally suggest that an 0900 albedo is, relative to other local times, the most representative of the diurnal average.

A second example concerns the Nimbus-7 earth radiation budget data (Kyle et al., 1986), which again refer to a sun-synchronous orbit, but with a noon equator crossing time. Here assuming a near-noon albedo to be the diurnal average would produce significant errors, with a corresponding sampling error in absorbed solar radiation (i.e., combining diurnally averaged insolation with a noon albedo) of as much as 20 W m^{-2} (Minnis and Harrison, 1984; Ramanathan, 1987). Consequently a diurnal correction factor, which we will later discuss, has been incorporated into the Nimbus-7 data reduction procedure (Kyle et al., 1986).

In contrast to sun-synchronous satellites, geostationary satellites, such as GOES and METEOSAT, constitute platforms from which earth radiation budget measurements may be made throughout the diurnal cycle (e.g., Minnis and Harrison, 1984; England and Hunt, 1984), but with a corresponding restriction as to geographical domain. Moreover, with respect to climate models Hansen et al. (1983), Randall et al. (1985), and Cess and Potter (1987) have all emphasized the importance of the diurnal cycle within three-dimensional general circulation models (GCMs), and this raises the question as to how to test diurnal processes conveniently within such models. One obvious candidate for this purpose would be to compare diurnal

Corresponding author address: Dr. R. D. Cess, Laboratory for Planetary Atmospheres Research, State University of New York, Stony Brook, NY 11794.

variability of the planetary albedo, as predicted by a GCM, to satellite measurements of this variability.

The purpose of the present paper is twofold. First, an atmospheric radiation model will be employed to illustrate several features associated with modeling the diurnal cycle of the planetary albedo. Following this, both satellite data and GCM results will be utilized as vehicles for understanding physical processes associated with diurnal variability of the planetary albedo, as well as addressing the issue of sampling errors inherent in albedo measurements made from sun-synchronous satellites. For this purpose Nimbus-7 will be employed as a convenient case in point.

2. Directional clear-sky albedo modeling

Obviously a key ingredient in modeling the diurnal variability of the planetary albedo is to express properly the dependence of the albedo upon solar zenith angle, and we first address this issue with respect to the clear-sky albedo. For this purpose we adopt the solar radiation model which is contained within the Oregon State University/Lawrence Livermore National Laboratory general circulation model (OSU/LLNL GCM). This is a delta-Eddington model which incorporates the near-infrared bands of water vapor, stratospheric ozone, Rayleigh scattering, and within which various atmospheric aerosols may be incorporated (Cess and Potter, 1986).

Model-predicted variations of the planetary albedo $\alpha(\mu)$, as a function of μ = cos(solar zenith angle), are illustrated in Fig. 1 for clear-sky conditions and for three surface types, where the albedo has been normalized to its overhead-sun value $\alpha(1)$. As in the OSU/LLNL GCM, the directional surface albedo, $\alpha_s(\mu)$, for ocean surfaces is that given by Briegleb et al. (1986). Other surface types are assumed to be Lambertian (i.e., no dependence upon μ), with $\alpha_s = 0.25$ for deserts. The OSU/LLNL GCM employs several different land surface categories (Ghan et al., 1982), with a composite $\alpha_s = 0.15$ being chosen here.

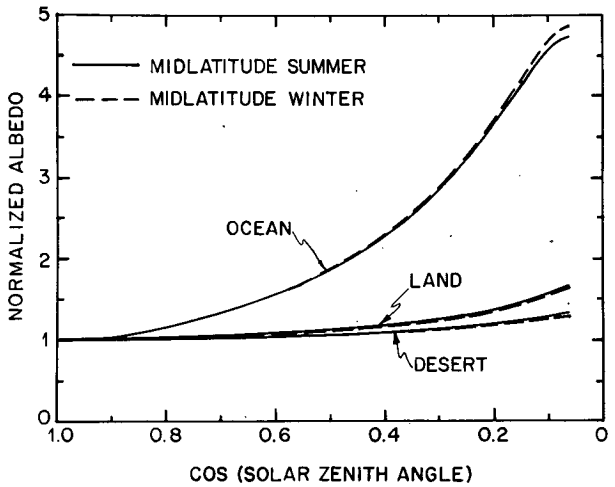

FIG. 1. Directional planetary albedos as evaluated from the solar radiation model utilizing both midlatitude summer and midlatitude winter water vapor abundances.

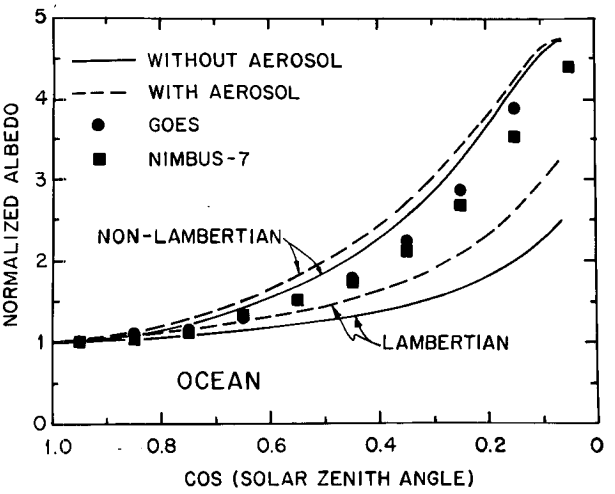

FIG. 2. Directional planetary albedos as evaluated from the solar radiation model both with and without maritime aerosols, and with and without the assumption of a Lambertian surface. Also shown are satellite results determined from both GOES (Minnis and Harrison, 1984) and Nimbus-7 (Taylor and Stowe, 1986) measurements.

The midlatitude summer and winter designations in Fig. 1 refer to the use of GCM-generated zonal-mean water vapor abundances for July and latitudes 42°N (summer) and 42°S (winter), with these different abundances having little effect upon the directional dependence of $\alpha(\mu)$. This by itself is important. For example, the directional albedo models utilized within the data reduction procedure for the Earth Radiation Budget Experiment (ERBE) refer solely to surface type; i.e., they are otherwise independent of location and season. The results of Fig. 1 thus suggest that this neglect of geographical and seasonal variations in atmospheric water vapor content is reasonable.

But the results of Fig. 1 ignore two potentially significant effects, namely, tropospheric aerosols and the μ dependence of α_s for land surfaces, the importance of both having been emphasized by Briegleb et al. (1986). To illustrate their potential impacts upon $\alpha(\mu)/\alpha(1)$, we first incorporate the maritime aerosol model of Briegleb et al. (1986) over ocean surfaces; this was accomplished by placing the aerosol within the model's lowest half-layer (800–1000 mb). Model results for $\alpha(\mu)/\alpha(1)$, both for a Lambertian surface and utilizing the directional surface albedo formulation (non-Lambertian) of Briegleb et al. (1986), are shown in Fig. 2, and for the non-Lambertian surface the aerosol only slightly enhances the dependence upon μ.

This is at first rather surprising, since it is well known that backscattering by such an aerosol increases with increasing solar zenith angle, producing a significant increase in atmospheric reflectivity with decreasing μ

(e.g., see Fig. 4 of Coakley et al., 1983). But how this in turn effects the planetary albedo depends upon α_s. For example, over a bright surface aerosol backscattering will have little impact upon the planetary albedo since that albedo is already large. What is happening, in contrast to the Lambertian surface, is that as solar zenith angle increases, the zenith-angle dependence of α_s produces a brighter ocean surface with thus a concurrent partial compensation in the effect of aerosol backscattering upon the planetary albedo.

However this near compensation refers only to the normalized albedo $\alpha(\mu)/\alpha(1)$. With respect to absolute albedos, Briegleb et al. (1986) have demonstrated that incorporation of maritime aerosols is necessary in order to achieve modeled albedos that agree with the GOES albedo measurements over ocean surfaces.

Also shown in Fig. 2 are directional albedo results determined from both GOES (Minnis and Harrison, 1984) and Nimbus-7 (Taylor and Stowe, 1986) measurements. The two datasets produce fairly comparable results and suggest a somewhat weaker dependence of $\alpha(\mu)$ upon μ than predicted by the models having a non-Lambertian surface, while differing considerably from those for which a Lambertian surface is assumed.

The non-Lambertian ocean-surface albedo of Briegleb et al. (1986) that we employ is based upon measurements made by Payne (1972) in Buzzards Bay, on the southeastern coast of Massachusetts, for a surface wind speed of 4 m s^{-1}. But measurements (e.g., Payne, 1972; Kondravt'ev, 1973) indicate that the dependence of α_s upon μ diminishes with increasing wind speed, and this raises the possibility that 4 m s^{-1} is too low a surface wind speed to be representative of the "global ocean".

To be more specific on this point, we additionally employ the ocean albedo model of Hansen et al. (1983), for which

$$\alpha = 0.021 + 0.0421x^2 + 0.1283x^3 - 0.04x^4 + \frac{3.12x^5}{5.68 + v} + \frac{0.074x^6}{1 + 3v} \quad (1)$$

where $x = 1 - \mu$ and v is the surface wind speed (m s^{-1}). This parameterization is based upon calculations of Fresnel reflection from wave surface distributions as a function of surface wind speed (Cox and Munk, 1956). In Fig. 3 we compare directional planetary albedos, as calculated using Eq. (1) with $v = 4$ and 15 m s^{-1}, to those employing the $v = 4$ m s^{-1} ocean albedo model of Briegleb et al. (1986). A surface wind speed of 15 m s^{-1} is excessive with respect to typical mean ocean conditions, and surface wind speed exerts a rather minor role, a conclusion likewise reached by Briegleb (personal communication, 1987) employing Payne's (1972) data. Note also the excellent agreement between use of the Hansen et al. (1983) and Briegleb et al. (1986) ocean albedo models for $v = 4$ m s^{-1}.

Also shown in Fig. 3 are the Nimbus-7 measurements. Since the GOES measurements agree reasonably well with those of Nimbus-7 (Fig. 2), they are not separately shown here. Clearly the impact of surface wind speed upon ocean albedo, as we presently understand it, does not explain the differences shown in Figs. 2 and 3 between the modeled (non-Lambertian) and measured directional planetary albedos.

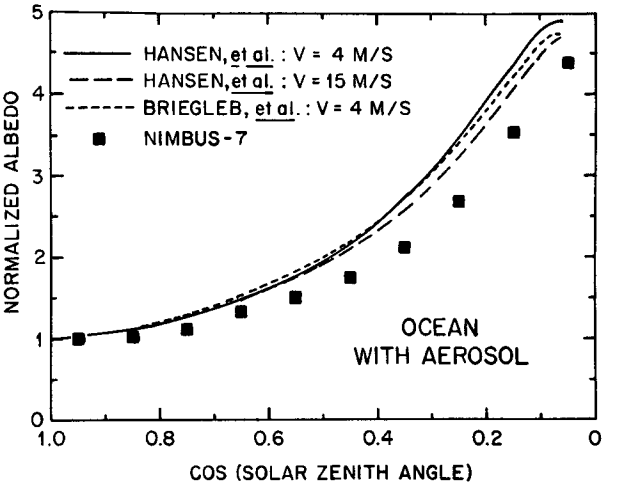

FIG. 3. Directional planetary albedos as evaluated from the solar radiation model using both Hansen et al. (1983) and Briegleb et al. (1986) albedo models for the ocean surface. Also shown are Nimbus-7 (Taylor and Stowe, 1986) measurements.

Turning next to land areas, it has been emphasized by Briegleb et al. (1986) that there is difficulty in attempting to model the albedo of land surfaces, and to further illustrate this point with regard to directional albedos, we have adopted a hierarchy of models. Model I refers to the land result of Fig. 1, where gray denotes that the surface albedo is not a function of wavelength. In model II we incorporate a wavelength dependence for α_s in the following manner. The solar spectrum in the radiation model encompasses three wavelength intervals: 0–0.5 μm, 0.5–0.9 μm and 0.9–5.0 μm, and within these respective intervals $\alpha_s = 0.04$, 0.0838 and 0.30, which represent a rough composite for the land surface types summarized by Briegleb et al. (1986). When integrated over the solar spectrum this yields $\alpha_s = 0.15$, consistent with model I.

Model III additionally incorporates the directional surface albedo of Briegleb et al. (1986),

$$\alpha_s(\mu) = \alpha_s(0.5)\frac{(1 + d)}{(1 + 2d\mu)}, \quad (2)$$

for which they employ $d = 0.1$ or 0.4 depending upon land surface type, while we adopt $d = 0.25$ as a composite value. Sensitivity studies indicate that our subsequent conclusions are not significantly dependent upon this choice of d. Model IV additionally incorporates tropospheric aerosols by using the same continental aerosol model as Briegleb et al. (1986) and, as

with maritime aerosols, incorporating the aerosol within the 800–1000 mb half-layer of the model.

An intercomparison of the four models is shown in Fig. 4, from which it is seen that the wavelength dependence of α_s has little impact upon the present problem. But this is not the case with respect to incorporating the μ-dependence of α_s (model III) and subsequently continental aerosols (model IV).

As in Fig. 2, we have also included within Fig. 4 both GOES and Nimbus-7 results which, unlike the prior comparison, are not in agreement. The reason for this is by no means clear, although there are at least two possible sources of disagreement. The GOES spin-scan radiometer is a narrowband instrument that has been calibrated by using the Nimbus-7 broadband scanner measurements as a reference. This was accomplished by employing near simultaneous, colocated radiance measurements taken for comparable solar and satellite zenith angles and relative azimuth angles (Minnis and Harrison, 1984). Thus the differences between the GOES and Nimbus-7 results shown in Fig. 4 might possibly be an artifact of this calibration procedure, although recall that such differences do not occur over ocean surfaces (Fig. 2). A second possible cause of the discrepancy may be differences in geographical coverage. Because of its noon orbit, Nimbus-7 only views higher latitudes (>45°) at high solar zenith angles (>60°) and tropics and midlatitudes at low solar zenith angles. The GOES results, on the other hand, include multiple views of the same areas for most solar zenith angles, but only for a limited portion of the globe.

Clearly Figs. 2, 3 and 4 illustrate inconsistencies in our knowledge of directional albedo modeling. Furthermore, to illustrate how these translate into uncertainties in the planetary albedo's diurnal cycle, a diurnal amplitude factor is defined as

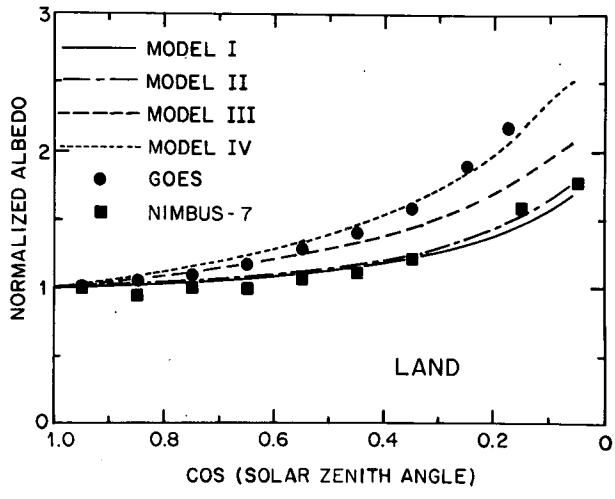

FIG. 4. Directional planetary albedos as evaluated from the solar radiation model for the four land/atmosphere models. Also shown are satellite results determined from both GOES (Minnis and Harrison, 1984) and Nimbus-7 (Taylor and Stowe, 1986) measurements.

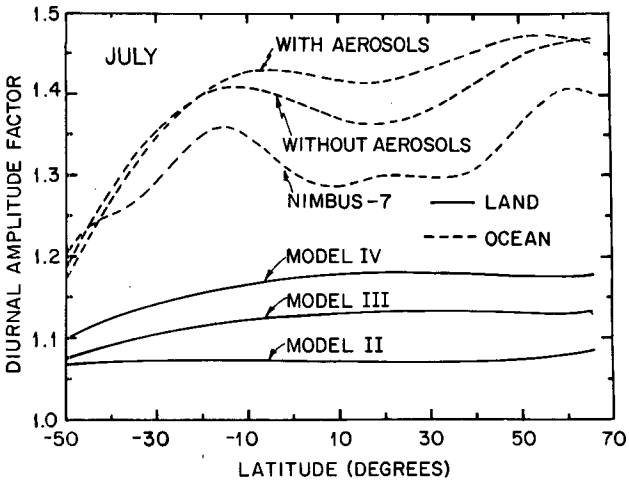

FIG. 5. Diurnal amplitude factors corresponding to directional albedo models shown in Figs. 2 and 4. The ocean models (with and without aerosols) refer to a non-Lambertian surface.

$$\text{Diurnal amplitude factor} = \frac{\alpha(\text{diurnal average})}{\alpha(\text{noon})}. \quad (3)$$

Within the context of Nimbus-7, which has a noon equator crossing time, this quantity essentially represents the diurnal correction factor (Kyle et al., 1986) by which the Nimbus-7 local-time albedo is converted to a diurnal average.

For comparative purposes, diurnal amplitude factors have been calculated as a function of latitude and for a July declination angle. These results are summarized in Fig. 5, and they were evaluated by employing the expression

$$\alpha(\text{diurnal average}) = \left(\frac{1}{2} H\bar{\mu}\right) \int_{-H}^{H} \alpha(h)\mu(h)dh, \quad (4)$$

where h is the hour angle, H is the half-day length, and $\bar{\mu}$ is the diurnal average of μ. For the Nimbus-7 data, Eq. (4) was evaluated by utilizing a polynomial fit to the Nimbus-7 results shown in Fig. 2. The solar radiation model, in conjunction with GCM-generated zonal-mean water vapor abundances for July, was employed to obtain the other results. Over ocean areas, only the non-Lambertian surface models of Fig. 2 have been considered.

The point of Fig. 5 is that the differences shown in Figs. 2 and 4 translate into quite sizable impacts upon the amplitude of the planetary albedo's diurnal cycle. A particularly perplexing issue is the fact that the Nimbus-7 directional albedo results over land most closely coincide with model II (see Fig. 4), which neither contains continental aerosols nor incorporates a dependence of the surface albedo upon solar zenith angle.

Although this section has been restricted to clear-sky albedos, which by themselves present obvious problems, clouds impact diurnal variability in two ways. First, there is the question of directional albedo models for overcast regions, which will most likely be

dependent upon cloud type. And second, both seasonal and diurnal variability in cloud structure and amount will exert an impact upon the diurnal cycle of the planetary albedo. To help explain these issues, in the following section two GCMs, in conjunction with GOES data, are employed as vehicles for elucidating several aspects of the diurnal amplitude factor.

3. GCM simulations

In this section we employ both the OSU/LLNL GCM (Cess and Potter, 1986, 1987) and the National Center for Atmospheric Research gridpoint GCM (Ramanathan, 1987) to illustrate certain features of the planetary albedo's diurnal cycle. The latter model (NCAR GCM) should not be confused with the current NCAR Community Climate Model (NCAR CCM), which is a spectral model that does not presently employ a diurnal cycle. Although the OSU/LLNL GCM is a two-level model, through interpolation four vertical cloud layers are actually formed within the model (Ghan et al., 1982; Cess et al., 1985). Our goal here is twofold: to understand physical processes associated with diurnal variability of the planetary albedo, as well as to illustrate how these processes impact sampling errors associated with converting a measured noon albedo to a diurnal average.

For this latter purpose we additionally adopt the correction factor used to convert the Nimbus-7 wide field-of-view measurements to diurnal-average albedos. This correction factor is essentially the same quantity as our diurnal amplitude factor. It was developed by A. Arking (see Kyle et al., 1986), and it consists of a global factor which depends solely upon latitude and solar declination angle. The Nimbus-3 directional albedo models of Raschke et al. (1973) were employed, using ocean and cloud/land subdivisions, with 90% weight given to the cloud/land model, since it was estimated that 90% of the reflected solar radiation stems from cloud/land regions. This correction factor thus makes no distinction between land versus ocean areas, nor does it account for seasonal and diurnal cloud variability. Because of these limitations, it thus serves as a useful comparison baseline for the purpose of elucidating the importance of land/ocean contrasts and of cloud variability.

A further resource for the purpose of understanding diurnal variability of the planetary albedo is the GOES dataset of Minnis and Harrison (1984) which, as discussed in the Introduction, encompasses the diurnal cycle, although with restriction as to geographical domain. This dataset is for a single month (November 1978) and refers to a region bounded by 45°S to 45°N, 30°W to 125°W, corresponding to the field of view of GOES-EAST.

In Fig. 6 diurnal amplitude factors are compared as determined from the GOES data, the Nimbus-7 correction factor, and the OSU/LLNL GCM. Two results are shown for the latter, one referring to zonal averages over the same longitudes as for the GOES measurements, and the second comprising zonal means over all longitudes.

Note first the reasonably good agreement that exists between the OSU/LLNL GCM (GOES longitudes) and the GOES data, which suggests that the GCM might well be a useful tool for studying diurnal variability of the planetary albedo. But there are caveats that must be appended to this conclusion, since agreement in gross quantities can often be a consequence of compensating differences in individual quantities. A case in point is the study by Cess and Potter (1987), in which top-of-the-atmosphere solar and infrared fluxes, as predicted by the OSU/LLNL GCM, were found to be in reasonable agreement with the GOES measurements of Minnis and Harrison (1984). This agreement, however, was actually a consequence of compensating differences, within the GCM, between cloud amount on the one hand, and overcast radiative fluxes on the other hand.

A similar situation occurs here. The GCM significantly underpredicts cloud cover relative to the November GOES data (Cess and Potter, 1987). Since, as will be shown, the GCM predicts a greater diurnal amplitude factor for clear as opposed to overcast regions, then this by itself should result in the GCM overestimating, relative to the GOES data, the diurnal amplitude factor. While Fig. 6 indicates that to some extent this is the case, there is a partially compensating effect in that the GCM correspondingly underestimates the diurnal amplitude factor for overcast regions, as is shown in Fig. 7. If this were not the case, then the overestimate in Fig. 6 would be substantially larger.

There are also compensatory differences with respect to the clear results shown in Fig. 7. For example, with reference to Figs. 2 and 4, and noting that the GCM simulation does not incorporate maritime aerosols, while over land areas it coincides with model I, then relative to the GOES data the GCM should overestimate the diurnal amplitude factor over oceans while

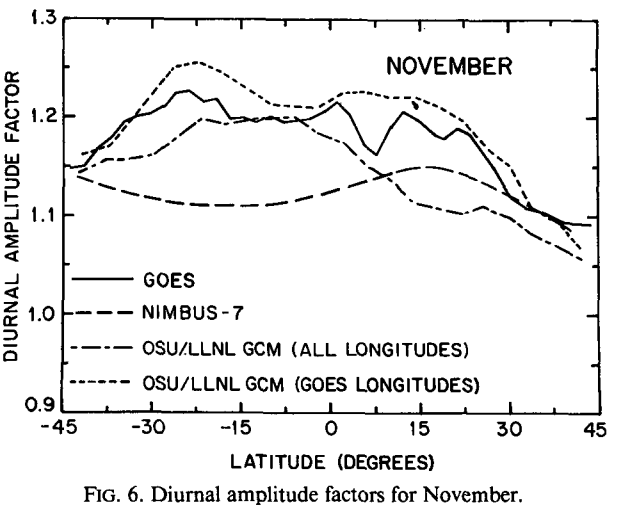

FIG. 6. Diurnal amplitude factors for November.

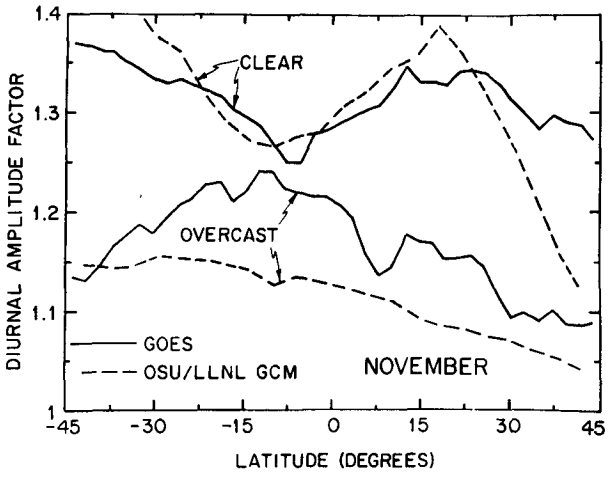

FIG. 7. Diurnal amplitude factors for November and for clear and overcast regions. The OSU/LLNL GCM results refer to GOES longitudes.

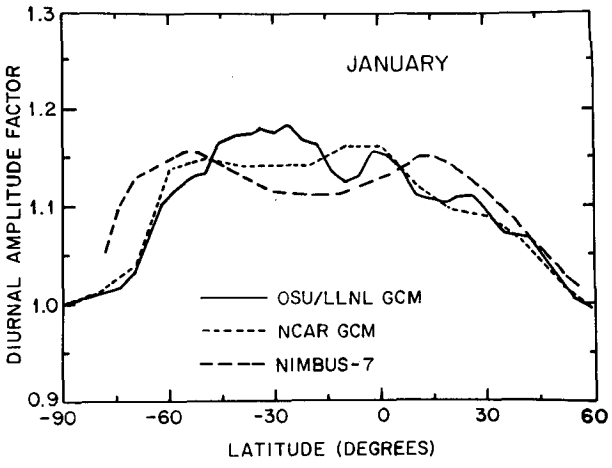

FIG. 8. Diurnal amplitude factors for January. These refer to all longitudes.

underestimating it over land. Inspection of the GCM output, together with GOES data, indeed confirms this, and such differences are in fact evident within Fig. 7. In the vicinity of latitude 15°N the only land area within the GOES field of view is Central America, and due to this predominance of ocean surface, here the GCM overestimates the diurnal amplitude factor relative to the GOES results. A similar effect is evident between 25°S and 45°S, where the South American landmass narrows to less than 10° of longitude. But at 42°N, North America encompasses half of the GOES field of view, with the GCM significantly underestimating the diurnal amplitude factor, consistent with its underestimate over land surfaces. For latitudes between 10°N and 25°S, on the other hand, the land/ocean ratios are such that these differences are more nearly compensatory.

Returning to Fig. 6, note that the GCM result for all longitudes is quite different than that for the GOES longitudes, and in part this again is traceable to different land/ocean ratios, coupled with the fact that the diurnal amplitude factor is greater over ocean areas. For example, the largest difference occurs for latitudes where only a small amount of land (Central America) is contained within the GOES field of view, whereas over all longitudes there are much greater land/ocean ratios due to the presence of Eurasia, and consequently at these latitudes the diurnal amplitude factor is significantly smaller than for the GOES longitudes. This emphasizes the importance of surface type upon the planetary albedo's diurnal cycle.

The final point of Fig. 6 is that there is a rather significant difference between the Nimbus-7 correction factor, which is a global quantity, and the GCM result referring to all longitudes. But this difference is dependent upon season, and as shown in Fig. 8 it is substantially reduced for January.

Also shown in Fig. 8 are results using the NCAR GCM, with the two GCMs being in quite good agreement. But this agreement should be viewed with some degree of caution since, as with the comparison between the OSU/LLNL GCM and the GOES data, it may be a consequence of compensatory differences. In that the NCAR GCM is no longer an operational model, it is not possible to further pursue this point.

The seasonal dependence of differences between the Nimbus-7 correction factor and the OSU/LLNL GCM is further illustrated by the July comparison shown in Fig. 9. Here the GCM produces much greater latitudinal variability than for January (Fig. 8). The reasons for this are due to corresponding differences in both seasonal and diurnal cloud cover, with neither of these effects being included in the Nimbus-7 correction factor.

For example, the GCM produces, for low and mid-latitudes, much greater latitudinal variability in zonal-mean cloud amount for July as opposed to January, a

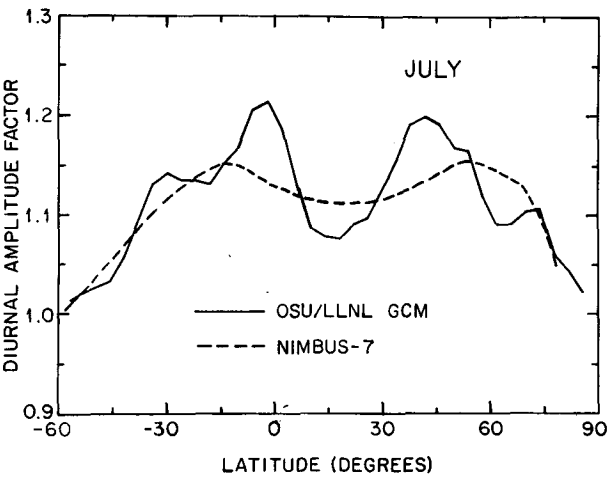

FIG. 9. As in Fig. 8 except for July.

result which is consistent with the satellite measurements of Stowe et al. (1986). Moreover, the July latitudinal variability of the GCM cloud cover is inversely correlated with the latitudinal variability of the diurnal amplitude factor as shown in Fig. 9. Since overcast regions produce a smaller diurnal amplitude factor than do clear regions (Fig. 7), then the enhanced July versus January ITCZ cloudiness is partially responsible for the pronounced tropical minimum shown in Fig. 9, with the reverse effect explaining, in part, the subtropical maxima.

4. Concluding remarks

One conclusion of the present study is that even for clear regions there exist deficiencies in our knowledge as to how to model the directional planetary albedo, with the most notable deficiency pertaining to land surfaces. The agreement between the Lambertian surface model and the Nimbus-7 data is particularly perplexing, since there is ample evidence that land surface albedos are dependent upon solar zenith angle (e.g., Monteith, 1975). This inconsistency is eliminated if we were to instead adopt the GOES data shown in Fig. 4, and it would seem most important to sort out the differences between these two datasets. Over ocean areas, on the other hand, the GOES and Nimbus-7 data are in agreement, and they produce a weaker dependence of the planetary albedo upon solar zenith angle than suggested by model studies.

Furthermore, we emphasize that we have utilized both satellite data and GCMs solely for the purpose of identifying important physical processes associated with diurnal variability of the planetary albedo. Given the possible uncertainties of the GOES data over land surfaces, together with the problem of compensatory differences within the OSU/LLNL GCM, we certainly do not interpret the agreement between the GCM and the GOES results, as shown in Fig. 6, to constitute validation of the model's diurnal cycle.

What the results of the present study do indicate is that diurnal variability of the planetary albedo is strongly dependent upon season due to cloud interactions. With respect to converting albedo measurements made from sun-synchronous orbits to diurnal averages, simple global correction factors, such as employed in the Nimbus-7 data reduction procedure, do not account for these cloud interactions. Nor do they allow for differences in scene type, such as land versus ocean, while the present study clearly illustrates the importance of such distinctions.

Acknowledgments. This work was partially performed under the auspices of the CO_2 Research Division, Office of Basic Energy Sciences, U.S. Department of Energy, under Contract W-7405-ENG-48 to Lawrence Livermore National Laboratory and Grant DEFG0285ER60314 to SUNY Stony Brook, and it was supported in part by the National Aeronautics and Space Administration through Contract NAS 1-18155 to SUNY Stony Brook and Contract NAS 1-18385 to the University of Chicago.

REFERENCES

Briegleb, B. P., P. Minnis, V. Ramanathan and E. Harrison, 1986: Comparison of regional clear-sky albedos inferred from satellite observations and model computations. *J. Climate Appl. Meteor.*, **25,** 214–226.

Cess, R. D., and G. L. Potter, 1986: Narrow- and broadband measurements of shortwave radiation: Conversion simulations with a general circulation model. *J. Climate Appl. Meteor.*, **25,** 1977–1984.

——, and ——, 1987: Exploratory studies of cloud radiative forcing with a general circulation model. *Tellus,* **39A,** 460–473.

Coakley, J. A., R. D. Cess and F. B. Yurevich, 1983: The effect of tropospheric aerosols on the earth's radiation budget: A parameterization for climate models. *J. Atmos. Sci.*, **40,** 116–138.

Cox, C., and W. Munk, 1956: Slopes of the sea surface deduced from photographs of the sun glitter. *Bull. Scripps. Inst. Oceanography,* **6,** 401–488.

England, C. F., and G. E. Hunt, 1984: A study of the errors due to temporal sampling of the earth's radiation budget. *Tellus,* **36B,** 303–316.

Ghan, S. J., J. W. Lingaas, M. E. Schlesinger, R. D. Mobley and W. L. Gates, 1982: A Documentation of the OSU Two-Level Atmospheric General Circulation Model. Rep. 61, Climatic Research Institute, Oregon State University, 391 pp.

Gruber, A., and J. S. Winston, 1978: Earth–atmosphere radiative heating based on NOAA scanning radiometer measurements. *Bull. Amer. Meteor. Soc.*, **59,** 1570–1573.

Hansen, J., G. Russel, D. Rind, P. Stone, A. Lacis, S. Lebedeff, R. Ruedy and L. Travis, 1983: Efficient three-dimensional global models for climate studies: Models I and II. *Mon. Wea. Rev.*, **111,** 609–662.

Kondrat'ev, K. Ya., 1973: *Radiation Characteristics of the Atmosphere and the Earth's Surface.* NASA TT 71-58003, 580 pp.

Kyle, H. L., K. L. Vasanth and the Nimbus-7 ERB Experiment Team, 1986: Some characteristic differences in the earth's radiation budget over land and ocean derived from the Nimbus-7 ERB experiment. *J. Climate Appl. Meteor.*, **25,** 958–981.

Minnis, P., and E. F. Harrison, 1984: Diurnal variability of regional cloud and clear-sky radiative parameters derived from GOES data. Part III: November 1978 radiative parameters. *J. Climate Appl. Meteor.*, **23,** 1032–1051.

Monteith, J. L., 1975: *Vegetation and the Atmosphere, Vol. I: Principles.* Academic Press, 278 pp.

Payne, R. E., 1972: Albedo of the sea surface. *J. Atmos. Sci.*, **29,** 959–970.

Ramanathan, V., 1987: The role of earth radiation budget studies in climate and general circulation research. *J. Geophys. Res.,* (in press).

Randall, D. A., J. A. Abeles and T. G. Corsetti, 1985: Seasonal simulations of the planetary boundary layer and boundary-layer stratocumulus clouds with a general circulation model. *J. Atmos. Sci.*, **42,** 641–676.

Raschke, E., T. H. Vonder Haar, M. Pasternak and W. R. Bandeen, 1973: The radiation balance of the earth–atmosphere system from Nimbus-3 radiation measurements. [NASA TN D-7249.]

Stowe, L. L., P. P. Pellegrino, P. H. Hwang, P. K. Bhartia, T. F. Eck and C. S. Long, 1986: Spatial and temporal characteristics of global cloud cover as observed from the Nimbus-7 satellite. Extended Abstracts, *Sixth Conf. on Atmospheric Radiation,* Amer. Meteor. Soc., Williamsburg, 99–102.

Taylor, V. R., and L. L. Stowe, 1986: Revised reflectance and emission models from Nimbus-7 ERB data. Extended Abstracts, *Sixth Conf. on Atmospheric Radiation,* Amer. Meteor. Soc., Williamsburg, J19–J22.